Vayá Pérez, I.; Andreu Ros, MI.; Lence, E.; González-Bello, C.; Cuquerella Alabort, MC.; Navarrete-Miguel, M.; Roca-Sanjuán, D.... (2020). Characterization of Locally Excited and Charge-Transfer States of the Anticancer Drug Lapatinib by Ultrafast Spectroscopy and Computational Studies. Chemistry - A European Journal. 26(68):15922-15930. https://doi.org/10.1002/chem.202001336

FULL PAPER

Characterization of the locally excited and charge-transfer states of the anticancer drug lapatinib by ultrafast spectroscopy and computational studies

Ignacio Vayá,*[a,b] Inmaculada Andreu,[a,b] Emilio Lence,[c] Concepción González-Bello,[c] M. Consuelo Cuquerella[a,b] Miriam Navarrete-Miguel,[d] Daniel Roca-Sanjuán,[d] Miguel A. Miranda*[a,b]

[a,b] Dr. I. Vayá, Dr. I. Andreu, Dr. M. C. Cuquerella, Prof. Dr. M. A. Miranda
Departamento de Química/Instituto de Tecnología Química UPV-CSIC
Universitat Politècnica de València
Camino de Vera s/n, 46022 València (Spain)
Unidad Mixta de Investigación UPV-Instituto de Investigación Sanitaria (IIS) La Fe
Hospital Universitari i Politècnic La Fe
Avenida de Fernando Abril Martorell 106, 46026, Valencia (Spain)
E-mail: mmiranda@qim.upv.es; igvapre@qim.upv.es
[c] Dr. E. Lence, Dr. C. González-Bello
Centro Singular de Investigación en Química Biolóxica e Materiais Moleculares (CiQUS), Departamento de Química Orgánica
Universidade de Santiago de Compostela
Jenaro de la Fuente s/n, 15782 Santiago de Compostela (Spain)
[d] M. Navarrete-Miguel, Dr. D. Roca-Sanjuán
Instituto de Ciencia Molecular
Universitat de València
P.O. Box 22085, 46071 València (Spain)

Supporting information for this article is given via a link at the end of the document

Abstract: Lapatinib (LAP) is an anticancer drug, which is metabolized to the N- and O-dealkylated products (N-LAP and O-LAP, respectively). In view of the photosensitizing potential of related drugs, a complete experimental and theoretical study has been performed on LAP, N-LAP and O-LAP, both in solution and upon complexation with human serum albumin (HSA). In organic solvent, coplanar locally excited (LE) emissive states are generated; they rapidly evolve towards twisted intramolecular charge-transfer (ICT) states. By contrast, within HSA only LE states are detected. Accordingly, femtosecond transient absorption reveals a very fast switching (ca. 2 ps) from LE (λ_{max} = 550 nm) to ICT states (λ_{max} = 480 nm) in solution, whereas within HSA the LE species become stabilized and live much longer (up to the ns scale). Interestingly, molecular dynamics simulation studies confirm that the coplanar orientation is preferred for LAP (or to a lesser extent N-LAP) within HSA, explaining the experimental results.

Introduction

According to the World Health Organization, breast cancer has become in 2018 the second leading cause of death worldwide.[1] The epidermal growth factor receptor (EGFR) is a transmembrane protein belonging to the same family as tyrosine kinase receptors HER2, HER3, and HER4, which controls a variety of cell functions including cell differentiation, proliferation, apoptosis, migration and angiogenesis.[2] Pathological alterations of EGFR and HER2, including kinase-activating mutation or overexpression, may result in the appearance of different types of cancer, such as pancreatic, colon, kidney or breast cancer.[3]

Lapatinib (LAP, see Scheme 1) is a synthetic, orally-active quinazoline with antineoplastic properties. It is the first dual inhibitor of EGFR and HER2 and was approved by the FDA in 2007.[4] The mechanism of LAP action involves binding to the adenosine triphosphate site, increasing apoptosis and reducing cellular proliferation.[5] It is also known that LAP binds strongly to albumin (>99%) and undergoes extensive metabolism in humans to give numerous oxidized, as well as N- and O-dealkylated products (N-LAP and O-LAP, respectively, Scheme 1). Indeed, it is known that O-LAP remains active against EGFR but not against HER2.[4a]

The binding of drugs to transport proteins has been widely investigated, due to its importance in the pharmacological action of the drug in the organism. Thus, processes such as drug solubility, toxicity and in vivo half-life are modulated through drug@protein complexation.[6] Besides, interaction of these complexes with light may result in photosensitivity disorders. For this reason, an extensive research effort has been devoted to understand the photosensitizing side effects mediated by the interaction of biomolecule-bound drugs with light.[7] In fact, drugs containing the quinazoline moiety are known to elicit skin diseases such as photodermatitis.[8]

Spectroscopic techniques, such as fluorescence and transient absorption, are very useful to investigate drug/protein interactions as they allow full characterization of the excited states involved in photosensitization. Thus, fluorescence is a highly sensitive technique, widely used in the steady-state and time-resolved modes to study the structural and dynamic features of drug@protein complexation. Likewise, ultrafast transient absorption spectroscopy is a powerful tool that can provide key information on the excited state dynamics at very short times, as they are known to be very sensitive to the microenvironment. Accordingly, the very fast photo-initiated processes such as intersystem crossing as well as energy or charge-transfer can significantly vary depending on the surroundings of the investigated chromophore.[7e]

Previous reports on the interaction of LAP with human serum albumin (HSA) have evidenced static quenching of the intrinsic protein emission, allowing the calculation of a binding constant of *ca.* 10^4 M^{-1}. Based on preliminary theoretical calculations in combination with fluorescence experiments using selective site probes it has been proposed that LAP mainly interacts in the so-called site III (subdomain IB) of HSA.[9] With this background, and with the aim to obtain a deeper insight into LAP@HSA binding, steady-state and time-resolved fluorescence as well as ultrafast transient absorption studies, in addition to detailed computational analysis on the chromophore including multiconfigurational quantum-chemistry calculations (complete-active-space self-consistent field/complete-active-space second-order perturbation theory CASSCF/CASPT2), have been undertaken. Moreover, the studies have been extended to the main LAP metabolites namely N-LAP and O-LAP, as they retain to some extent the photosensitivity and/or pharmacological properties of the parent drug.

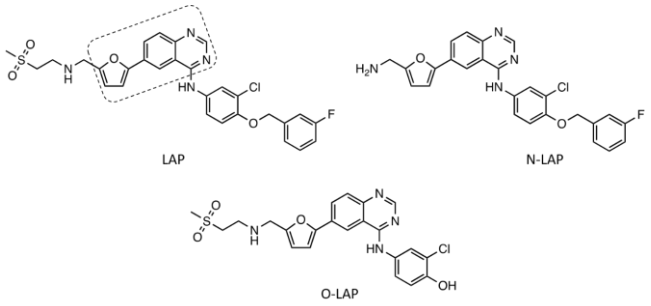

Scheme 1. Chemical structures of lapatinib (LAP) and its main metabolites N-LAP and O-LAP. The dashed frame shows the LAP simplified model containing the central π-conjugated chromophores for CASSCF/CASPT2 computational analysis.

Results and Discussion

The photophysical properties of LAP were first investigated in organic solution. The emission of the drug in MeCN and ethanol was very low at room temperature, in agreement with previous observations in methanol.[9c] However, the fluorescence was dramatically enhanced in a solid ethanol matrix at 77K (see Figures S1 and S2 in the Supporting Information). This effect can be attributed to the restriction in the degrees of freedom for conformational relaxation in the frozen medium, which could prevent a possible intramolecular charge-transfer (ICT), similar to that previously observed for related drugs.[10]

The photobehavior of LAP was also investigated in aqueous medium and in the presence of human serum albumin (HSA). In PBS LAP is known to form aggregates;[9c] this is clearly shown by the UV absorption spectra (see Figure S3 in the Supporting Information). However, in the presence of HSA at 1:1 molar ratio (10 μM), the drug was completely solubilized (see Figure S4 in the Supporting Information). Hence, steady-state fluorescence measurements were performed on isoabsorptive solutions at two excitation wavelengths (295 or 340 nm).

Emission of LAP@HSA at λ_{exc} = 295 nm, where both the protein and the drug absorb light, is shown in Figure 1A. Under these conditions, a clear quenching of the intrinsic protein fluorescence centered at 340 nm was observed. Interestingly, while the emission of LAP in PBS was unstructured and very minor due to aggregation, the profile changed dramatically within the protein binding sites; here, the fluorescence of the drug was strongly enhanced, and the shape of the spectrum was more structured and shifted towards shorter wavelengths (from 470 to 425 nm). This effect is very similar to that observed between EtOH at 298 K and 77 K and can be attributed to the solid matrix effect, in addition to the blockage of a possible ICT process. Thus, incorporation of LAP to HSA not only avoids aggregation favoring its solubility, but it likewise enhances its fluorescence due to the more constrained microenvironment that may also help to block the charge-transfer process.

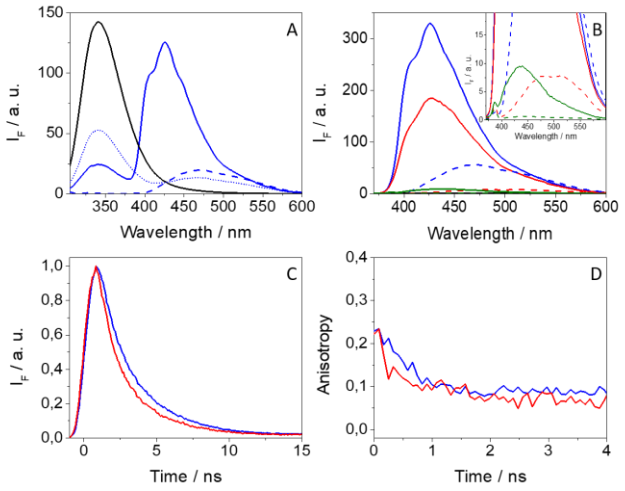

Figure 1. (A) Fluorescence spectra of HSA (black), LAP (dashed blue) and LAP@HSA at 1:1 molar ratio (solid blue) in PBS under air, using isoabsorptive solutions at λ_{exc} = 295 nm. The simulated emission of LAP@HSA, determined as explained elsewhere[11] taking into account the percentage of photons absorbed by HSA and LAP at 295 nm, and considering no interaction between the two entities, is shown in dotted blue. (B) Emission of LAP (dashed blue), N-LAP (dashed red), O-LAP (dashed green), LAP@HSA (blue), N-LAP@HSA (red) and O-LAP@HSA (green) at 1:1 molar ratio in PBS under air, using isoabsorptive solutions at λ_{exc} = 340 nm. The inset shows a zoom of the lower fluorescence spectra. (C) Fluorescence decay traces and (D) anisotropy decays for LAP@HSA (blue) and N-LAP@HSA (red) at 1:1 molar ratio upon excitation at 340 nm in aerated PBS.

The emission of LAP within HSA upon excitation at 295 nm may not only arise from the direct absorption of light but also from energy transfer with the protein as donor due to spectral overlap (see Figure S5A in the Supporting Information). This process, which is dynamic in nature, is supported by the femtosecond transient absorption results (see below).

Fluorescence experiments at λ_{exc} = 295 nm were also done with the main metabolites N-LAP and O-LAP. As it can be clearly observed from Figure S6 in the Supporting Information, interaction of both metabolites with HSA was much weaker than that of LAP. For N-LAP, a moderate quenching of the protein emission attributable to singlet-singlet energy transfer (SSET) was detected, while in the case of O-LAP such quenching was insignificant. Indeed, the percentages of decrease of the protein emission centered at 340 nm upon interaction with LAP, N-LAP and O-LAP were determined to be 54%, 37% and 13%, respectively.

Selective excitation of the protein bound drug (or metabolite) at 340 nm evidenced the highest fluorescence yield for LAP (Figure 1B); yet, emission from N-LAP was lower and less structured than that of the parent drug, indicating weaker interaction with HSA, while emission from O-LAP either in PBS or within the protein was nearly undetectable. This can be associated with a lower contribution of ICT states for LAP than for both metabolites within the protein. In addition, the negligible fluorescence of O-LAP may also be related to an alternative deactivation pathway involving deprotonation of the phenol moiety in the excited state. Figure 1C displays the fluorescence decay traces for LAP or N-LAP within HSA, from which a somewhat shorter lifetime was determined for the metabolite ($<\tau> = 1.2$ ns) than for LAP itself ($<\tau> = 1.5$ ns); this is in line with the steady-state results. Besides, anisotropy decays (Figure 1D) evidenced a tight interaction of the drug and the metabolite with the protein; thus, LAP@HSA and N-LAP@HSA decay from r_0 *ca.* 0.22 to a constant value close to 0.1 within 0.53 and 0.46 ns, respectively, confirming a huge restriction in the degrees of freedom for conformational relaxation of the drug, or to a lesser extent the metabolite, within the protein.

With the aim of characterizing in more detail the photobehavior of LAP in the first steps upon interaction with light, femtosecond transient absorption measurements in acetonitrile and in PBS, in the presence of HSA at different excitation wavelengths, were performed. In the organic solvent, transient absorption spectra during the first 5 ps after excitation at 330 nm (Figure 2A) showed an instantaneous formation of two bands centered at 550 and 400 nm that rapidly evolved towards a new absorption band around 480 nm, through two isosbestic points at *ca.* 420 and 510 nm; the 480 nm transient started to decay at longer times (Figure 2B).

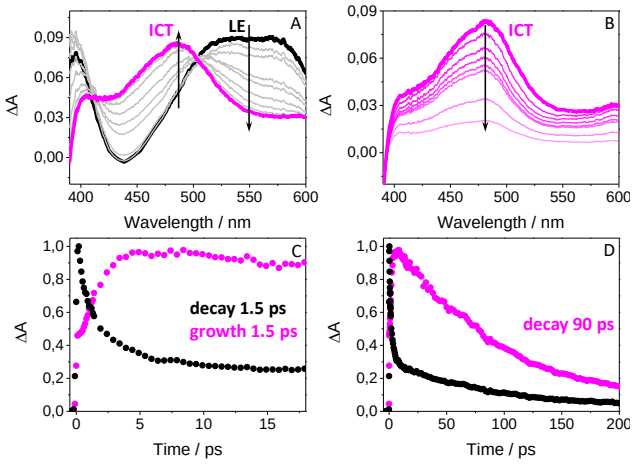

Figure 2. Femtosecond transient absorption measurements for LAP in acetonitrile upon excitation at 330 nm: spectra from (A) 0.5 (black) to 5 ps (magenta) and (B) from 5 to 150 ps; decay traces at 550 (black) and 480 nm (magenta) at two different time windows: 18 ps (C) and 200 ps (D).

Analysis of the decay traces at 400 and 550 nm showed that both transient bands disappear in a parallel way; two components were necessary to get a good fitting, with lifetimes of *ca.* 90 ps and *ca.* 1.5 ps. Interestingly, the shorter one matches with that obtained in the formation of the trace at 480 nm (see Figure 2C). Thus, the band centered at 550 nm is assigned to the singlet-singlet absorption of LAP, that rapidly evolves (≈ 1.5 ps) to another state, attributed to the abovementioned ICT state, which displays a maximum at 480 nm and decays with a lifetime of *ca.* 90 ps (see Figure 2D). A similar behavior was detected for N-LAP, but with different kinetics; in this case, the evolution from the locally excited singlet state to ICT is accomplished in *ca.* 1.9 ps, which decays in about 70 ps (see Figure S7 in the Supporting Information).

By contrast with the light absorbing species detected in MeCN, the scenario observed in the LAP@HSA (or N-LAP@HSA) complexes evidenced formation of only one transient species assigned to the singlet-singlet absorption band, with maxima *ca.* 420 and 530 nm. For LAP@HSA, its decay followed a second order law with two components with lifetimes of *ca.* 12 ps and almost 1 ns (see Figure 3), while for N-LAP@HSA the shorter component was found to be of about 8.5 ps, while the longer one lasted again up to the ns scale (see Figure S8 in the Supporting Information). It is worth to note that ICT formation was blocked within the protein cavities, which provide a constrained microenvironment less polar and more lipophilic than the bulk aqueous medium.

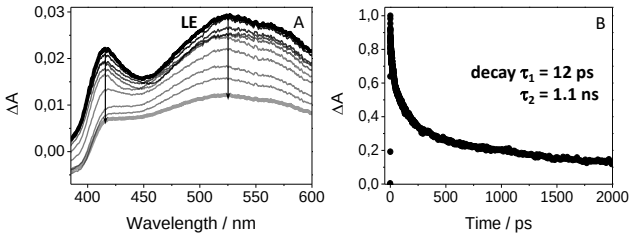

Figure 3. (A) Femtosecond transient absorption spectra from 1 to 200 ps, and (B) decay trace monitored at 530 nm for LAP@HSA at 1:1 molar ratio (3×10^{-4} M) in PBS, using 330 nm as excitation wavelength.

Having discussed the ultrafast dynamics after excitation of the LAP@HSA complexes at 330 nm, where LAP is the only light absorbing species, it is interesting to come back to the point mentioned above regarding the emission from the complexes upon excitation at $\lambda < 300$ nm, when both protein and drug absorb light. Under these conditions, LAP fluorescence can result from both direct absorption of light by the drug and SSET process from HSA to LAP. As a matter of fact, ultrafast transient absorption measurements for LAP@HSA upon 280 nm laser excitation (see Figure S5B in the Supporting Information) evidenced instantaneous formation of the band with maximum centered at *ca.* 530 nm, assigned to ^{1}LAP*, together with a delayed (650 fs) growth that occurred up to *ca.* 900 fs; the latter was assigned to the formation of ^{1}LAP* through SSET from the excited Trp residue of the protein.

In order to further characterize the excited states generated after light absorption by the drug (or its metabolites), a computational analysis was performed on the central π-conjugated system containing the furan and quinazoline chromophores present in LAP, N-LAP and O-LAP (see Scheme 1, dotted frame). The secondary amine of LAP breaks the conjugation, so the excitation process is mainly driven by the furan and quinazoline rings. Such reduction of the molecular size allowed us to carry out a high-level CASSCF/CASPT2[12] analysis of the electronic structure properties for the ground and excited states, which is required for a proper description of localized and charge-transfer states.

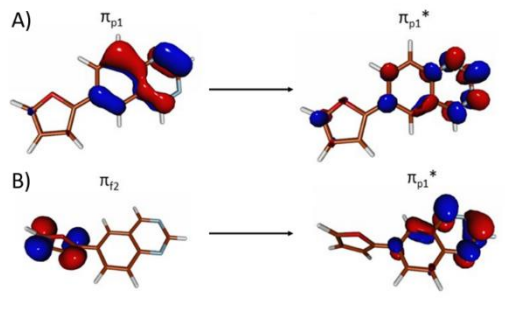

Figure 4. Main electronic excitations characterizing the photophysics of LAP simplified model at the coplanar (A) and twisted (B) structures.

Based on the herein reported experimental findings pointing to two relevant excited states and the possible involvement of an ICT with large structural changes, the electronic ground and excited states were characterized at two structures A and B (Figure 4) with a coplanar orientation of the furan and quinazoline rings and with 90º-twisted geometry, respectively. Tables S1 and S2 in the Supporting Information compile the electronic transition data for both structures. At the coplanar arrangement, all the low-lying excited states correspond to excitations localized in the quinazoline part, the S_4 state displaying the brightest electronic transition, with a vertical energy of 4.73 eV (Figure 4A). None of the computed states have a significant charge-transfer character as indicated by the values of the dipole moments and the orbital excitations related to each state (see Figure S9 in the Supporting Information). In fact, no charge-transfer state was predicted even when computing 20 excited states. Such scenario changes upon twisting the furan and quinazoline parts (see Figure S10 in the Supporting Information). As can be seen in Table S2 in the Supporting Information, a new relevant state appears at 5.30 eV (S_7 state) with a much higher dipole moment (μ) than that of the ground state (S_0), which corresponds to a charge-transfer excitation from the furan ring to the quinazoline moiety (Figure 4B). Based on the obtained data and the previous analyses, the photophysical properties of LAP at short times after absorbing light should be governed by the excited state localized in the quinazoline part with a coplanar orientation with the furan ring (as in the ground state equilibrium geometry). This state evolves towards the charge-transfer state *via* a twisting of the middle single bond which is associated with the growing transient absorption signal appearing in the experimental spectra. The charge-transfer state must therefore govern the photophysics at longer times.

Further insights into the relative arrangement of the furan and quinazoline rings in LAP and its metabolites when binding to HSA, along with the interactions responsible for that arrangement, were obtained by Molecular Dynamics (MD) simulation studies. The binding mode of the ligands to subdomain IB was initially explored by Molecular Docking using the program GOLD 5.7.0[13] and the protein coordinates found in the crystal structure of HSA in complex with hemin (PDB entry 1O9X),[14] which binds to subdomain IB. The resulting ligand@HSA binary complexes were submerged in a truncated octahedron of water molecules and further analyzed by MD simulations using the molecular mechanics force field AMBER.[15] This type of studies in which both the ligand and the protein are flexible: (i) allows discarding false binding modes; and (ii) gives a more realistic conformation of the ligand and the ligand@protein complex (induced-fit model). The two possible protonation states of the secondary and primary amino groups in the ligands were initially considered. However, the neutral forms of the ligands were ruled out based on the higher stability of their protonated forms in the pocket during the simulations.

The results of these MD simulation studies revealed that the proposed binding for LAP and its metabolites in subdomain IB obtained by docking was feasible as the complexes proved to be stable during the simulation. The root-mean-square deviation (rmsd) for the whole protein backbone (C^{α}, C, N and O atoms) calculated in the three complexes revealed to be low (see Figure S11 in the Supporting Information). For the LAP@HSA complex, the results showed that: (i) only one conformation among those existing in solution for LAP is selected when bound to subdomain IB of HSA; and (ii) this conformation is frozen by the protein. Thus, selective inversion NOE experiments with LAP in deuterated methanol showed a 1:1.9 ratio of the two possible rotamers around the furan-quinazoline bond, being the major conformer the one in which the oxygen atom of the furan ring is located on the same side as the amino group in the quinazoline ring (see Figure S12 in the Supporting Information). As shown in Figures 5A and 5B, the major conformation obtained in solution is selected by HSA. More importantly, an almost coplanar arrangement of the furan and quinazoline rings was observed during the whole simulation. Thus, the analysis of the dihedral angle between the furyl (oxygen and C2´ atoms) and quinazoline (C5´ and C4´ atoms) moieties in LAP in the LAP@HSA binary complex during the simulation revealed that this coplanar arrangement is frozen by the protein as no significant changes were identified (Figure 5E). The average value of the dihedral angle is 7.85º for the last 80 ns of simulation. In view of the CASSCF/CASPT2 results, this arrangement would clearly favor emission from its locally excited singlet state, blocking the ICT process; this is in line with the experimental results shown above.

Thus, LAP would be anchored in subdomain IB by two strong hydrogen bonding interactions, one between the sulfone oxygen atom and the main NH group of Glu119, and another one between the main carbonyl group of Val116 and the amino group of the ligand, which is mediated by a water molecule (Figure 5B). These interactions were observed during 63% and 78% of the simulation, respectively. In addition, LAP would be stabilized in subdomain IB by numerous favorable non-polar interactions between the aromatic part of the ligand and the side chain residues within the pocket, specifically Met123, Phe134, Tyr138, Leu139, His146, Leu154, Phe157, Tyr161 and Phe165.

On the contrary, the binding mode of N-LAP in subdomain IB of HSA proved to be markedly different from LAP, evidencing a reverse binding of the main aromatic rings and, more importantly, with much less coplanarity between them (Figures 5C and 5D). The analysis of the variation of the aforementioned dihedral angle in N-LAP in the N-LAP@HSA binary complex during the whole simulation revealed a large rotation around the furan-quinazoline bond, with an average value of -59.5º for the last 80 ns of simulation (Figure 5F). This non-planar arrangement agrees with its lower emission within the protein. Moreover, the N-LAP different binding arrangement, its lower conformational restriction

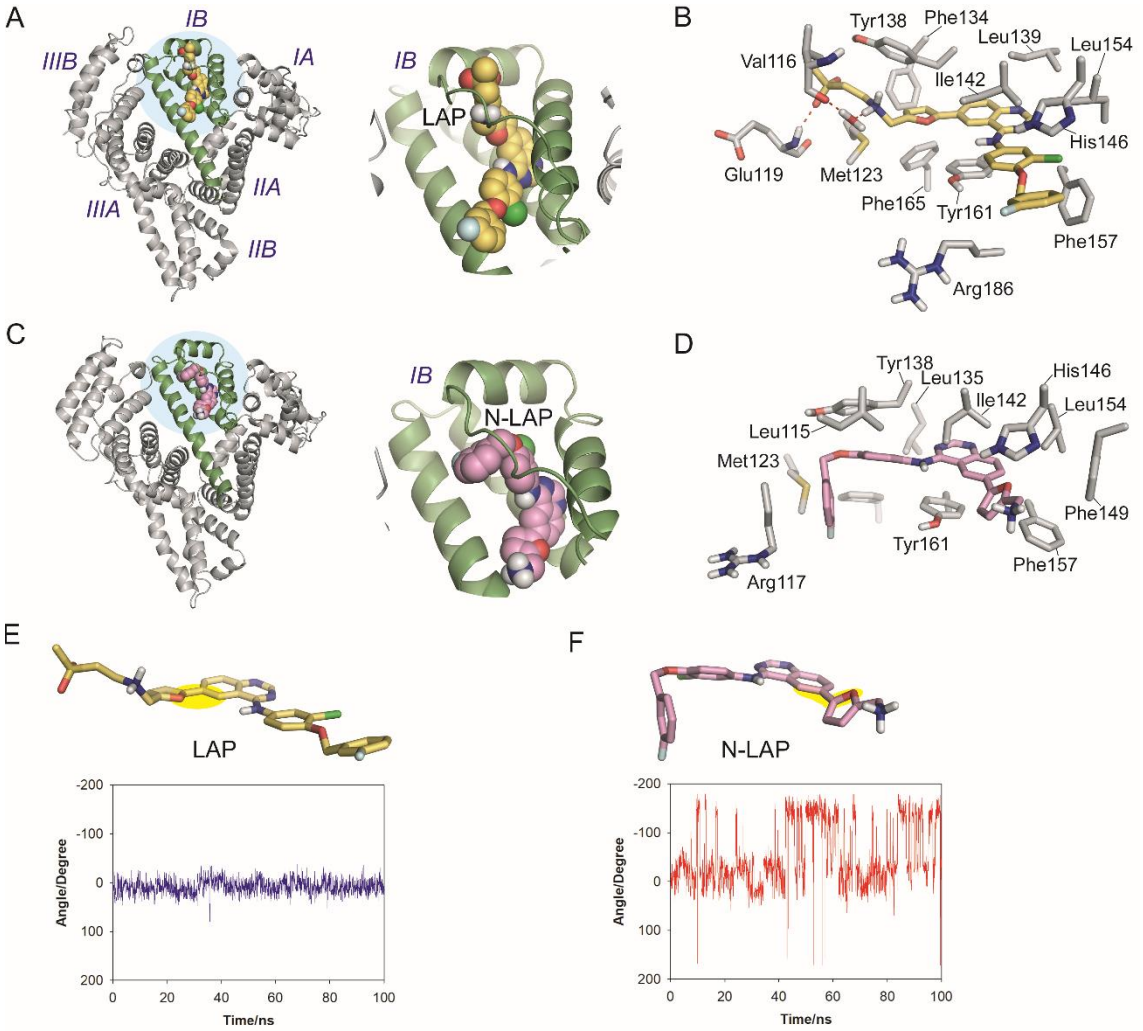

Figure 5. Binding mode of LAP (A-B) and N-LAP (C-D) with HSA protein obtained by MD simulation studies. (A,C) Overall views of the LAP@HSA (A) and N-LAP@HSA (C) binary complexes obtained by MD simulation studies. Snapshots after 60 ns are shown. The main backbone of LAP and N-LAP are shown as yellow and violet spheres, respectively. Relevant interactions of LAP (B) and N-LAP (D) with the subdomain IB of HSA. Note how the binding mode of LAP is markedly different from N-LAP. Hydrogen bonding interactions between the ligands and the protein are shown as red dashed lines. Relevant side chain residues are shown and labelled. (E-F) Variation of the dihedral angle between the furyl and quinazoline moieties of LAP (E) and N-LAP (F) in the LAP@HSA and the N-LAP@HSA protein complexes, respectively, during 100 ns of simulation. The bonds involved in the dihedral angle are highlighted with a yellow shadow.

achieved within the protein, as well as its smaller size might explain the enhancement of the fluorescence experimentally observed after addition of IBP or WRF, while they do not affect LAP emission. Thus, IBP and WRF might cause conformational changes in the neighboring subdomains that might contribute to push N-LAP to a more constrained environment.

In order to obtain experimental confirmation on the binding site of LAP or N-LAP inside the protein, selective site I or site II probes, such as warfarin (WRF)[16] or ibuprofen (IBP),[17] were used. Addition of either WRF or IBP to LAP@HSA resulted in no significant change in the emission of the drug within the protein. By contrast, for N-LAP@HSA both probes provoked an enhancement of the metabolite emission (see Figure S13 in the Supporting Information). Thus, it can be concluded that neither LAP nor N-LAP bind preferentially to site I or site II of HSA but to a different one. Interestingly, in the case of N-LAP, addition of the probes seems to generate greater constraint in the binding site, resulting in higher emission. This allosteric effect was previously observed with other drugs and site probes interacting with proteins, and it is mainly due to large conformational changes in the macromolecule upon ligand binding.[18]

Finally, the MD simulation studies carried out with the nearly non-emissive O-LAP@HSA binary complex revealed a similar binding mode to that of LAP (see Figure S14 in the Supporting Information). More importantly, the phenol group of the ligand would have the appropriate arrangement to be deprotonated by Glu425 (subdomain IIIA), acting as a general base. This deprotonation process would be mediated by a water molecule network and Lys190, which might explain the rapid deactivation.

Conclusion

The photophysical properties of LAP and their main metabolites, N-LAP and O-LAP, have been fully characterized in solution and in the presence of HSA by means of ultrafast spectroscopy,

multiconfigurational quantum-chemistry calculations and MD simulation studies. CASSCF/CASPT2 analysis reveals that the photobehavior of LAP upon interaction with light is initially governed by emissive excited states localized on the quinazoline and furan rings in a coplanar orientation, which evolve to twisted ICT states. This process has been experimentally confirmed by femtosecond transient absorption measurements; thus, a band centered at 550 nm is instantaneously formed upon excitation of LAP in MeCN, that progresses in about 1.5 ps to an ICT state ($\lambda_{max} \approx 480$ nm). Switching from locally excited to charge-transfer emitting states is also supported by steady-state fluorescence measurements in ethanol both in solution at room temperature and in a solid matrix. Thus, LAP does not display significant emission at 298 K, while a strong enhancement is observed at 77 K probably due to the blockage of ICT in the matrix. A similar behavior is evidenced in the protein-bound fluorophore, since the weak shapeless and red-shifted emission of LAP (or N-LAP) arising from aggregates in PBS is strongly enhanced and much more structured within the protein. This is due to a favored coplanar orientation between the furan and quinazoline moieties within the binding pockets, which is much higher for LAP than for N-LAP. Interestingly, MD simulation studies clearly explain this effect, showing that the detected emission increases with the decreasing dihedral angle between the quinazoline and furan rings. Finally, in addition to displacement experiments, simulation studies undoubtedly confirm subdomain IB of HSA as the high affinity binding site not only for LAP but also for its metabolites N-LAP and O-LAP.

Experimental Section

Chemicals and Reagents

Lapatinib (CAS 231277-92-2), ibuprofen, warfarin, and human serum albumin were purchased from Sigma-Aldrich (Madrid, Spain). N-De[2-(methylsulfonyl)ethyl lapatinib (N-LAP, CAS 697299-82-4) and O-De(3-fluorobenzyl) lapatinib ditosylate salt (O-LAP; CAS 1268997-70-1) were provided by Santa Cruz Biotechnology (Dallas, USA) and Toronto Research Chemicals (North York, Canada), respectively. PBS buffer was prepared by dissolving phosphate-buffered saline tablets (Sigma-Aldrich) using ultrapure water from a Millipore (Milli-Q Synthesis) system. Spectrophotometric HPLC solvents were obtained from Scharlab and used without further purification.

Spectroscopic Measurements

Steady-state absorption spectra were recorded in a JASCO V-760 spectrophotometer. Steady-state fluorescence spectra were obtained using a JASCO-8500 spectrofluorometer system provided with a monochromator in the wavelength range 200-900 nm, with an excitation wavelength of 295 or 340 nm at 25 ºC. Measurements on drug or metabolite@protein complexes were performed in aerated PBS of 1:1 molar ratio mixtures at 10 μM.

Time-resolved fluorescence measurements were done using an EasyLife X system containing a sample compartment composed of an automated peltier cuvette holder to control the temperature, a pulsed LED excitation source and a lifetime detector. The employed LED excitation source was 340 nm, with emission filter of GG400. Anisotropy decays were measured by controlling the polarization of the exciting beam with the corresponding polarizers. From the parallel and perpendicular measurements, the fluorescence anisotropy decay was calculated using the formula:

$$r(t) = \frac{I_{par}(t) - RI_{perp}(t)}{I_{par}(t) + 2RI_{perp}(t)}$$

The transmission under parallel and perpendicular conditions was found to be identical so the correction factor R was put to unity.

The UV and fluorescence measurements were recorded using 10 × 10 mm^2 or 10 × 4 mm^2 quartz cells at 25 ºC. The absorbance of the samples at the excitation wavelength was kept below 0.1. Fluorescence measurements in the solid matrix of ethanol were achieved by introducing the solution in a quartz tube of 5 mm of diameter and cooled with liquid N_2 (77 K).

Femtosecond transient absorption experiments were performed using a typical pump-probe system. The femtosecond pulses were generated with a mode-locked Ti-Sapphire laser of a compact Libra HE (4 W power at 4 kHz) regenerative amplifier delivering 100 fs pulses at 800 nm (1 mJ/pulse). The output of the laser was split into two parts to generate the pump and the probe beams. Thus, tunable femtosecond pump pulses were obtained by directing the 800 nm light into an optical parametric amplifier. In the present case, the pump was set at 330 nm and passed through a chopper prior to focus onto a rotating cell (1 mm optical path) containing the samples in organic or aqueous solution. The white light used as probe was produced after part of the 800 nm light from the amplifier travelled through a computer controlled 8 ns variable optical delay line and impinge on a CaF_2 rotating crystal. This white light was in turn split in two identical portions to generate reference and probe beams that then are focused on the rotating cell containing the sample. The pump and the probe were made to coincide to interrogate the sample. A computer-controlled imaging spectrometer was placed after this path to measure the probe and the reference pulses to obtain the transient absorption decays/spectra. The experimental data were treated and compensated by the chirp using the ExciPro program.

Computational CASSCF/CASPT2 analysis

Ground state geometry optimization. The structure of the lapatinib simplified model (see Scheme 1) was optimized by means of the density functional (DFT) method with the B3LYP functional and the 6-31G* basis set as implemented in the GAUSSIAN 09 software package,[19] giving rise to the so-called coplanar structure. From the obtained geometry, the dihedral angle between the furan and quinazoline moieties was increased until 90º resulting in the so-called twisted structure. No significant differences for the geometrical parameters have been found by further optimizing the geometry with the M06-2X functional and the 6-311G* basis set (see Figure S15 in the Supporting Information).

Electronic transitions. The complete-active-space second-order perturbation theory (CASPT2) method[12] and the atomic natural orbital (ANO) S-type basis set with a contraction scheme C, N, O[3s,2p,1d]/H[2s1p], hereafter ANO-S-VDZP, were used as implemented in the MOLCAS 8 program[20] to determine the electronic structure properties of the ground and lowest-lying excited states at the coplanar and twisted geometries. Ten roots were averaged in the CASSCF computations [hereafter, SA(10)-CASSCF]. The most relevant π, π* and nitrogen lone pair (nN) orbitals were selected for the active space, which corresponds to a total of 14 active electrons distributed in 12 active orbitals. The dynamic electron correlation was computed using the CASPT2 method using the SA-CASSCF(14,12) wave functions. The ionization-potential electron-affinity parameter (IPEA) was set to the standard value of 0.00 au, which has been successful in many studies in similar molecular system with basis sets of the same quality.[21] An imaginary level shift of 0.2 au was used to minimize the presence of weakly intruder states.[22] Oscillator strengths (*f*) were calculated according to the formula $f = (2/3)E\,TDM^2$, where *E* stands for the CASPT2 vertical absorption energy, and TDM refers to the transition dipole moment between the initial φ_1 and final φ_2 SA-CASSCF wave functions, according to the formula $TDM = \langle\varphi_1|\vec{\mu}|\varphi_2\rangle$, where $\vec{\mu}$ is the dipole moment operator.

Molecular Docking

These calculations have been performed using GOLD 5.7.0 program[13] and the protein coordinates were taken from the crystal structure of HSA in complex with hemin (PDB entry 1O9X).[14] The experimental procedure was similar to that described for 2-acetoxy-4-trifluoromethylbenzoic acid (triflusal),[7b] with the exception that the position of hemin was used to define the binding pocket, and the radius was set to 10 Å. The protonated forms of the ligands (secondary and primary amines) were employed.

Molecular Dynamics Simulation Studies

The highest score solution obtained by docking was subjected to 100 ns of dynamic simulation. The experimental protocol involved: (i) the minimization of the ligands (LAP, N-LAP and O-LAP); (ii) the generation and minimization of the binary LAP@HSA, N-LAP@HSA, and O-LAP@HSA protein complexes using the poses obtained by docking; and (iii) MD simulations of the resulting minimized ligand@HSA complexes. The protocol was performed as described for triflusal.[7b] The analysis of the trajectories and the rmsd of the atomic positions of the protein and the ligands during the simulation were analyzed by using the cpptraj module in AMBER 16.[15] The protein figures disclosed were created by using the molecular graphics program PyMOL.[23]

Acknowledgements

Financial support from the Spanish Government (RYC-2015-17737, CTQ2017-89416-R, ISCIII grants RD16/0006/0004, PI16/01877 and CPII16/00052, SAF2016-75638-R, RYC-2015-19234, CTQ2017-87054-C2-2-P, and MDM-2015-0538), Consellería d'Educació Cultura i Esport (PROMETEO/2017/075), the Xunta de Galicia [ED431B 2018/04 and Centro singular de investigación de Galicia accreditation 2019-2022 (ED431G 2019/03)] and the European Regional Development Fund is gratefully acknowledged. We thank the Centro de Supercomputación de Galicia (CESGA) for use of the Finis Terrae computer.

Conflict of interest

The authors declare no conflict of interest.

Keywords: CASSCF/CASPT2 • Femtosecond transient absorption • Fluorescence • Lapatinib • Molecular dynamics simulations

[1] F. Bray, J. Ferlay, I. Soerjomataram, R. L. Siegel, L. A. Torre and A. Jemal, *CA Cancer J. Clin.* **2018**, *68*, 394-424.

[2] a) R. I. Nicholson, J. M. W. Gee and M. E. Harper, *Eur. J. Cancer* **2001**, *37*, S9-S15; b) M. Yashiro, H. Qiu, T. Hasegawa, X. Zhang, T. Matsuzaki and K. Hirakawa, *Br. J. Cancer* **2011**, *105*, 1522-1532.

[3] a) G. González and A. Lage, *Curr. Cancer Drug Targets* **2007**, *7*, 229-241; b) S. Sigismund, D. Avanzato and L. Lanzetti, *Mol. Oncol.* **2018**, *12*, 3-20; c) R. Thomas and Z. Weihua, *Front. Oncol.* **2019**, *9*.

[4] a) P. J. Medina and S. Goodin, *Clin. Ther.* **2008**, *30*, 1426-1447; b) M. Nolting, T. Schneider-Merck and M. Trepel, *Recent Results Cancer Res.* **2014**, *201*, 125-143.

[5] a) R. L. Schroeder, C. L. Stevens and J. Sridhar, *Molecules* **2014**, *19*, 15196-15212; b) N. L. Spector, W. Xia, H. Burris, 3rd, H. Hurwitz, E. C. Dees, A. Dowlati, B. O'Neil, B. Overmoyer, P. K. Marcom, K. L. Blackwell, D. A. Smith, K. M. Koch, A. Stead, S. Mangum, M. J. Ellis, L. Liu, A. K. Man, T. M. Bremer, J. Harris and S. Bacus, *J. Clin. Oncol.* **2005**, *23*, 2502-2512.

[6] a) J. Krasner, *Pediatr. Clin. North Am.* **1972**, *19*, 51-63; b) T. Peters in *Ligand binding by albumin*, (Ed. Elsevier), Academic Press, San Diego, **1995**, pp. 76-132.

[7] a) O. Molins-Molina, E. Lence, D. Limones-Herrero, C. González-Bello, M. A. Miranda and M. C. Jiménez, *Org. Chem. Front.* **2019**, *6*, 99-109; b) O. Molins-Molina, R. Perez-Ruiz, E. Lence, C. Gonzalez-Bello, M. A. Miranda and M. C. Jimenez, *Front. Pharmacol.* **2019**, *10*, 1028; c) A. F. Monteiro, M. Rato and C. Martins, *Clin. Dermatol.* **2016**, *34*, 571-581; d) I. Vayá, I. Andreu, V. T. Monje, M. C. Jimenez and M. A. Miranda, *Chem. Res. Toxicol.* **2016**, *29*, 40-46; e) I. Vayá, V. Lhiaubet-Vallet, M. C. Jimenez and M. A. Miranda, *Chem. Soc. Rev.* **2014**, *43*, 4102-4122.

[8] a) T. Ishikawa, R. Kamide and M. Niimura, *J. Dermatol.* **1994**, *21*, 430-433; b) T. P. Selvam and P. V. Kumar, *Res. Pharm.* **2011**, *1*, 1-21.

[9] a) M. Z. Kabir, A. K. Mukarram, S. B. Mohamad, Z. Alias and S. Tayyab, *J. Photochem. Photobiol. B* **2016**, *160*, 229-239; b) G. F. Shen, T. T. Liu, Q. Wang, M. Jiang and J. H. Shi, *J. Photochem. Photobiol. B* **2015**, *153*, 380-390; c) J. N. Wilson, W. Liu, A. S. Brown and R. Landgraf, *Org. Biomol. Chem.* **2015**, *13*, 5006-5011.

[10] M. D. Li, Z. Yan, R. Zhu, D. L. Phillips, I. Aparici-Espert, V. Lhiaubet-Vallet and M. A. Miranda, *Chem. Eur. J.* **2018**, *24*, 6654-6659.

[11] I. Vayá, P. Bonancia, M. C. Jimenez, D. Markovitsi, T. Gustavsson and M. A. Miranda, *Phys. Chem. Chem. Phys.* **2013**, *15*, 4727-4734.

[12] a) K. Andersson, P. Malmqvist and B. O. Roos, *J. Chem. Phys.* **1992**, *96*, 1218-1226; b) K. Andersson, P. Å. Malmqvist, B. O. Roos, A. J. Sadlej and K. Wolinski, *J. Phys. Chem.* **1990**, *94*, 5483-5488; c) D. Roca-Sanjuán, F. Aquilante and R. Lindh, *Wiley Interdiscip. Rev. Comput. Mol. Sci.* **2012**, *2*, 585-603.

[13] in http://www.ccdc.cam.ac.uk/solutions/csd-discovery/components/gold/ (accessed January 22, 2020).

[14] P. A. Zunszain, J. Ghuman, T. Komatsu, E. Tsuchida and S. Curry, *BC Struct. Biol.* **2003**, *3*, 6.

[15] D. A. Case, R. M. Betz, D. S. Cerutti, T. E. Cheatham, T. A. Darden, R. E. Duke, T. J. Giese, H. Gohlke, A. W. Goetz, N. Homeyer, S. Izadi, P. Janowski, J. J. Kaus, A. Kovalenko, T. S. Lee, S. LeGrand, P. Li, C. Lin, T. Luchko, R. Luo, B. Madej, D. Mermelstein, K. M. M. Merz, G. Monard, H. Nguyen, H. Nguyen, I. Omelyan, A. Onufriev, D. R. R. Roe, A. Roitberg, C. Sagui, C. L. Simmerling, W. M. Botello-Smith, J. Swails, R. Walker, J. Wang, R. M. Wolf, X. Wu, L. Xiao and P. A. Kollman, *AMBER* **2016**, University of California, San Francisco.

[16] T. Wybranowski, M. Cyrankiewicz, B. Ziomkowska and S. Kruszewski, *Biosystems* **2008**, *94*, 258-262.

[17] T. Itoh, Y. Saura, Y. Tsuda and H. Yamada, *Chirality* **1997**, *9*, 643-649.

[18] R. Perez-Ruiz, E. Lence, I. Andreu, D. Limones-Herrero, C. Gonzalez-Bello, M. A. Miranda and M. C. Jimenez, *Chem. Eur. J.* **2017**, *23*, 13986-13994.

[19] M. J. Frisch, G. W. Trucks, H. B. Schlegel, G. E. Scuseria, M. A. Robb, J. R. Cheeseman, G. Scalmani, V. Barone, B. Mennucci, G. A. Petersson, H. Nakatsuji, M. Caricato, X. Li, H. P. Hratchian, A. F. Izmaylov, J. Bloino, G. Zheng, J. L. Sonnenberg, M. Hada, M. Ehara, K. Toyota, R. Fukuda, J. Hasegawa, M. Ishida, T. Nakajima, Y. Honda, O. Kitao, H. Nakai, T. Vreven, J. J. A. Montgomery, J. E. Peralta, F. Ogliaro, M. Bearpark, J. J. Heyd, E. Brothers, K. N. Kudin, V. N. Staroverov, R. Kobayashi, J. Normand, K. Raghavachari, A. Rendell, J. C. Burant, S. S. Iyengar, J. Tomasi, M. Cossi, N. Rega, J. M. Millam, M. Klene, J. E. Knox, J. B. Cross, V. Bakken, C. Adamo, J. Jaramillo, R. Gomperts, R. E. Stratmann, O. Yazyev, A. J. Austin, R. Cammi, C. Pomelli, J. W. Ochterski, R. L. Martin, K. Morokuma, V. G. Zakrzewski, G. A. Voth, P. Salvador, J. J. Dannenberg, S. Dapprich, A. D. Daniels, Ö. Farkas, J. B. Foresman, J. V. Ortiz, J. Cioslowski and D. J. Fox, *Gaussian 09, Revision D.01*, **2013** Wallingford, CT.

[20] F. Aquilante, J. Autschbach, R. K. Carlson, L. F. Chibotaru, M. G. Delcey, L. De Vico, I. Fdez. Galván, N. Ferré, L. M. Frutos, L. Gagliardi, M. Garavelli, A. Giussani, C. E. Hoyer, G. Li Manni, H. Lischka, D. Ma, P. Å. Malmqvist, T. Müller, A. Nenov, M. Olivucci, T. B. Pedersen, D. Peng, F. Plasser, B. Pritchard, M. Reiher, I. Rivalta, I. Schapiro, J. Segarra-Martí, M. Stenrup, D. G. Truhlar, L. Ungur, A. Valentini, S. Vancoillie, V. Veryazov, V. P. Vysotskiy, O. Weingart, F. Zapata and R. Lindh, *J. Comput. Chem.* **2016**, *37*, 506-541.

[21] a) D. Roca-Sanjuán, A. Francés-Monerris, I. F. Galván, P. Farahani, R. Lindh and Y. J. Liu in *Advances in computational photochemistry and chemiluminescence of biological and nanotechnological molecules*, *Vol. 44* **2017**, pp. 16-60; b) D. Roca-Sanjuán, I. Fdez. Galván, R. Lindh and Y. J. Liu in *Recent method developments and applications in computational photochemistry, chemiluminescene and bioluminescence*, *Vol. 42* **2015**, pp. 11-42.

[22] N. Forsberg and P.-Å. Malmqvist, *Chem. Phys. Lett.* **1997**, *274*, 196-204.

[23] W. L. DeLano in *The PyMOL Molecular Graphics System. http://www.pymol.org/*.

Entry for the Table of Contents

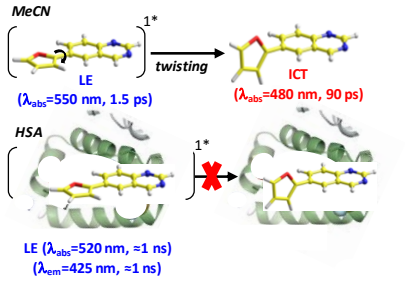

The photophysical properties of the anticancer drug lapatinib and two of its metabolites have been fully characterized in solution and in the presence of HSA by means of ultrafast spectroscopy and computational studies; all results point that the geometrical arrangement controls their photobehavior. Thus, in a coplanar orientation locally excited states are formed, while in a twisted positioning intramolecular charge-transfer states prevails.